Quantification of Gestational Changes in the Uteroplacental Vascular Tree Reveals Vessel Specific Hemodynamic Roles During Pregnancy in Mice[1]

Monique Y. Rennie,[3,4] Kathie J. Whiteley,[7] S. Lee Adamson,[4,5,6,7] and John G. Sled[2,3,4]

[3]Mouse Imaging Centre, Hospital for Sick Children, Toronto, Ontario, Canada
[4]Department of Medical Biophysics, University of Toronto, Toronto, Ontario, Canada
[5]Department of Obstetrics and Gynecology, University of Toronto, Toronto, Ontario, Canada
[6]Department of Physiology, University of Toronto, Toronto, Ontario, Canada
[7]Lunenfeld-Tanenbaum Research Institute, Mount Sinai Hospital, Toronto, Ontario, Canada

ABSTRACT

The purpose of this study was to establish the time course and hemodynamic significance of de novo formed and enlarged uteroplacental arteries during pregnancy. Using x-ray micro-computed tomography (n = 4–7 placentas from 2–4 dams/gestational group), uteroplacental arterial vascular dimensions were measured at individual implantation sites. Dimensions and topology were used to compute total and vessel-specific resistances and cross-sectional areas. Diameter enlargement of the uterine artery (+55% by Embryonic Day 5.5 [E5.5]) and preplacental radial arteries (+30% by E8.5) was significant only in early gestation. Formation of spiral arteries (E9.5–E11.5), maternal canals, and canal branches (E11.5–E13.5) during midgestation was followed by enlargement of these vessels such that, from E9.5 to E17.5 (near term), spiral artery resistance dropped 9-fold, and canal resistance became negligible. A 12-fold increase in terminal vessel cross-sectional area was nearly sufficient to offset known increases in flow so that blood velocity entering the exchange region was predicted to increase by only 2-fold. The calculated 47% decrease in total resistance downstream of the uterine artery, determined from vascular geometry, was in accord with prior uterine blood flow data in vivo and was due to enlarging spiral artery diameters. Interestingly, radial artery resistance was unchanged after E9.5 so that radial arteries accounted for 91% of resistance and pressure drop in the uteroplacental arterial network by E17.5. These findings led us to propose functional roles for the three morphologically defined vessel types: radial arteries to reduce pressure, spiral artery enlargement to increase flow with gestation, and maternal canal elaboration and enlargement to maintain low exit velocities into the exchange region.

hemodynamics, microcomputed tomography, mouse, placenta, resistance, uteroplacental circulation

INTRODUCTION

Insufficient remodeling of the uteroplacental vascular tree is suspected to underlie some of the most common and severe pregnancy complications, including miscarriage, intrauterine growth restriction, and pre-eclampsia [1, 2]. Yet, despite its undisputed importance in supporting a healthy pregnancy, there is a dearth of information on normal pregnancy-induced augmentation of this vascular bed, specifically on how variations in tree structure influence vascular resistance to blood flow and pressure drop across the vascular bed. Poor remodeling is believed to result in reduced uteroplacental blood flow, and reduced uteroplacental blood flow has been shown to elicit pre-eclamptic symptoms in animal models [3, 4]. However, the precise location of suspected defects remains elusive. Current dogma posits that pre-eclampsia stems from failure of the spiral arteries to be transformed into wide, flaccid tubes [1, 5], resulting in a higher, detrimental resistance to blood flow. Yet, biopsies from many pre-eclamptic women exhibit normal spiral artery remodeling [5]. Furthermore, blunted radial artery dilation has been observed in pre-eclamptic women [6]. Thus, the site of resistance changes in the uteroplacental circulation of both normal and pathological pregnancies remains unknown.

In humans, while the overall structure of the uteroplacental circulation is well understood, the limited spatial resolution of in vivo imaging techniques such as magnetic resonance imaging and ultrasound mean that less is known about the functional roles of the vessels and developmental dynamics across gestation. Uteroplacental tissue collection is limited to biopsies containing a small portion of this bed, usually one spiral artery at most [7]. Thus, minimal to no structural data exists pertaining to the time course of arcuate and radial artery vascular remodeling upstream of the spiral arteries [8, 9]. Clinically, changes in vascular resistance are identified via changes in the uterine artery Doppler waveforms and the calculated resistance or pulsatility indices [10], which seemingly reflect alterations in vascular structure downstream [11]. However, waveform changes and calculated indices do not reliably predict changes in vascular resistance [12] nor localize the site of a downstream resistance change [13, 14].

Mouse models present an opportunity to enhance understanding of uteroplacental vascular expansion, structure, and resistance during normal human pregnancy due to strong structural similarities of the uteroplacental circulation [15–17],

comparable uterine artery Doppler waveforms before and during pregnancy [18], and the wealth of mouse models available for the study of uteroplacental vascular pathology (e.g., [19–21]). Importantly, the small size of the mouse placenta enables ex vivo three-dimensional imaging of the entire, intact uteroplacental tree via microcomputed tomography (micro-CT) [19, 22]. The resulting high resolution images enable detection of site-specific uteroplacental vascular defects in various rodent models [19, 23, 24], computation of vascular resistance [19], and an understanding of how small changes in vascular structure can significantly alter resistances at each level of the tree [19]. Ultimately, the availability of genetic and environmentally induced mouse models of pre-eclampsia and fetal growth restriction (e.g., [19, 25–27]) promise greater understanding of the etiology of human pregnancy pathology. The goals of this study were 1) to use micro-CT imaging in the mouse to quantify arterial growth and remodeling within the uterine circulation from prepregnancy through to near full term and 2) to determine the effect of structural changes throughout pregnancy on site-specific vascular resistances to blood flow, pressure drops, and blood flow velocities.

MATERIALS AND METHODS

Mice

Experimental procedures were approved by the Animal Care Committees of Mount Sinai Hospital and the Toronto Centre for Phenogenomics and were conducted in accordance with guidelines established by the Canadian Council on Animal Care. CD-1 mice were purchased from Charles River Laboratories. Images of the nonpregnant uterine vasculature were obtained from 8- to 10-wk-old virgin females in estrus, which was initiated via priming the cage with male urine and confirmed through vaginal appearance [28, 29]. Males were mated in-house with 8- to 14-wk-old virgin females, and the morning that a vaginal copulation plug was detected was designated Embryonic Day 0.5 (E0.5). Uteroplacental vasculature was studied at E5.5, E8.5, E9.5, E11.5, E13.5, E15.5, and E17.5 of gestation.

Injection of Contrast Agent and CT Scanning

The uteroplacental vasculature was perfused with x-ray contrast agent using previously established methods [22, 30]. In brief, mice were anesthetized with isoflurane, and intracardiac heparin (0.05 ml at 100 IU/ml) was injected and allowed to circulate. A catheter in the descending thoracic aorta was used to clear the lower body vasculature of blood using pump-infused heparinized saline containing xylocaine as a vasodilator [22, 30, 31]. The pump then infused the contrast agent (HV-122 Microfil; Flow Tech Inc.). Infusion was stopped when the bright yellow color of the contrast agent was seen entering the uterine microvasculature (in nonpregnant females) or entering the uteroplacental microvasculature of the exposed pregnant uterus, thus generating samples in which only the arterial vasculature and microvessels contained the contrast agent. After tying off the inferior vena cava, the system was pressurized to 20 mm Hg (i.e., microvascular pressure [32]) while the compound polymerized. The uterus was then removed and immersed in formalin.

Three-dimensional datasets were acquired from agarose gel-mounted uteroplacental specimens using a micro-CT scanner (Model 1172; Skyscan). With the x-ray source at 50 kV and 201 μA, the specimen was rotated 180° in 0.4° increments, generating 480 views in 2 h that were reconstructed into data blocks with a 13.4 μm voxel size. Vascular surface renderings were generated from micro-CT data to visualize the arterial vasculature [33]. Uteroplacental canal, spiral artery, radial artery, and uterine artery luminal diameters and lengths were measured directly from these surface renderings using digital calipers in the software package (Amira; FEI Visualization Sciences Group). Three or more diameter measurements were made at intervals along each vessel type and then were averaged. Due to the large variation in spiral artery diameters within an implantation site, at least 15 spiral artery diameter measurements were averaged, making standard error of the mean values similar between vessel types.

Hemodynamic Modeling

Resistance calculations assumed 1) laminar flow, 2) Poiseuille's equations for flow of fluid through a pipelike structure, 3) conservation of mass (flow into a vessel = flow out of a vessel), and 4) equations for resistors in series ($R_{total} = R_1 + R_2 + \ldots$) and in parallel ($1/R_{total} = 1/R_1 + 1/R_2 + \ldots$). Measured vessel diameters and lengths were used to calculate vascular resistance for individual vessels using Poiseuille's law. Resistances of vascular networks were calculated using a combination of standard formulas for resistances in parallel and in series as described previously [19]. Total resistance of the arterial uteroplacental vascular tree was calculated from the number and the topology of radial arteries, spiral arteries, maternal canals, and maternal canal branches in each placenta. Resistance calculations were possible only from E9.5 onward, by which point specific vessel types within an implantation site were identifiable and reliable measurements of diameter, length, and vessel numbers could be obtained.

Blood flow through the maternal canals at each gestational age was calculated based on our measurements of canal number and diameter and time-averaged mean flow velocities. Gestational age-specific mean flow velocities were derived from ultrasound measurements of maternal canal peak systolic velocity, measured daily between E10.5 and E18.5 in the same strain of mice [18], by integrating the area under the curve for a set time interval. Within a single implantation site, blood flow was assumed to be the same at each level of the uteroplacental tree because the radial arteries, spiral arteries, and canals are in series. Therefore, we used calculated blood flow combined with measured resistance at each level of the uteroplacental circulation to estimate pressure drops ($\Delta P = Q \times R$), where ΔP (mmHg) is the pressure drop, Q (mm^3/sec) is the blood flow, and R (mmHg s μL^{-1}) is resistance. As maternal canal peak systolic velocity data is not available prior to E10.5, E11.5 was the earliest time point for which blood flow and pressure drop was computed. Blood flow was also combined with cross-sectional areas to calculate blood flow velocities at each level of the circulation (V = Q/A), where V (mm/sec) is the velocity, Q (mm^3/sec) is the blood flow, and A (mm^2) is the cross-sectional area.

Statistical Analysis

Statistical tests were performed using Prism (GraphPad Software, Inc). Data were analyzed using one-way ANOVA to evaluate the effect of gestational age. Where the ANOVA was significant ($P < 0.05$), Tukey post hoc tests were performed. Technical merit, based on the appearance of complete filling of the arterial vasculature by visual inspection of micro-CT datasets, was the sole criteria used to select placentas for quantitative analysis. The total number of dams analyzed at each time point was as follows: nonpregnant (6), E5.5 (3), E8.5 (2), E9.5 (2), E11.5 (3), E13.5 (4), E15.5 (3), E17.5 (4). In pregnant dams, between one and three placentas were analyzed from each litter, for a total number of implantation sites analyzed per group (n) as follows: E5.5 (4), E8.5 (4), E9.5 (4), E11.5 (5), E13.5 (8), E15.5 (7), E17.5 (8). All data are shown as mean ± SEM.

RESULTS

In the nonpregnant murine uterus, radial arteries branched from the uterine artery to feed the myometrial uterine wall (Fig. 1A). By E5.5, changes in the intrauterine microvasculature appeared to reveal implantation sites although specific vessel types were not identifiable at this early stage (Fig. 1B). Two types of radial arteries were distinguishable in micro-CT images by E8.5 and were clearly imaged at E9.5 (Fig. 1C). Premyometrial radial arteries supplied the myometrium, and preplacental radial arteries supplied implantation sites [34]. Downstream from preplacental radial arteries, spiral arteries and maternal canals developed de novo during gestation in the virgin mice studied here. Spiral arteries were visible on micro-CT images by E9.5 (Fig. 1C), at which point between five and nine spiral arteries were visible. Spiral arteries were small in diameter with minimal coiling (Fig. 1E). By E13.5, the spiral arteries had taken on the large diameter coiled geometry that is characteristic of these vessels (Fig. 1F). Maternal canals formed downstream of the spiral arteries by E11.5, at which point between two and five maternal canals had been established. By E13.5 canal branches were also present (Figs. 1D and 2B). These large diameter, trophoblast-lined vessels
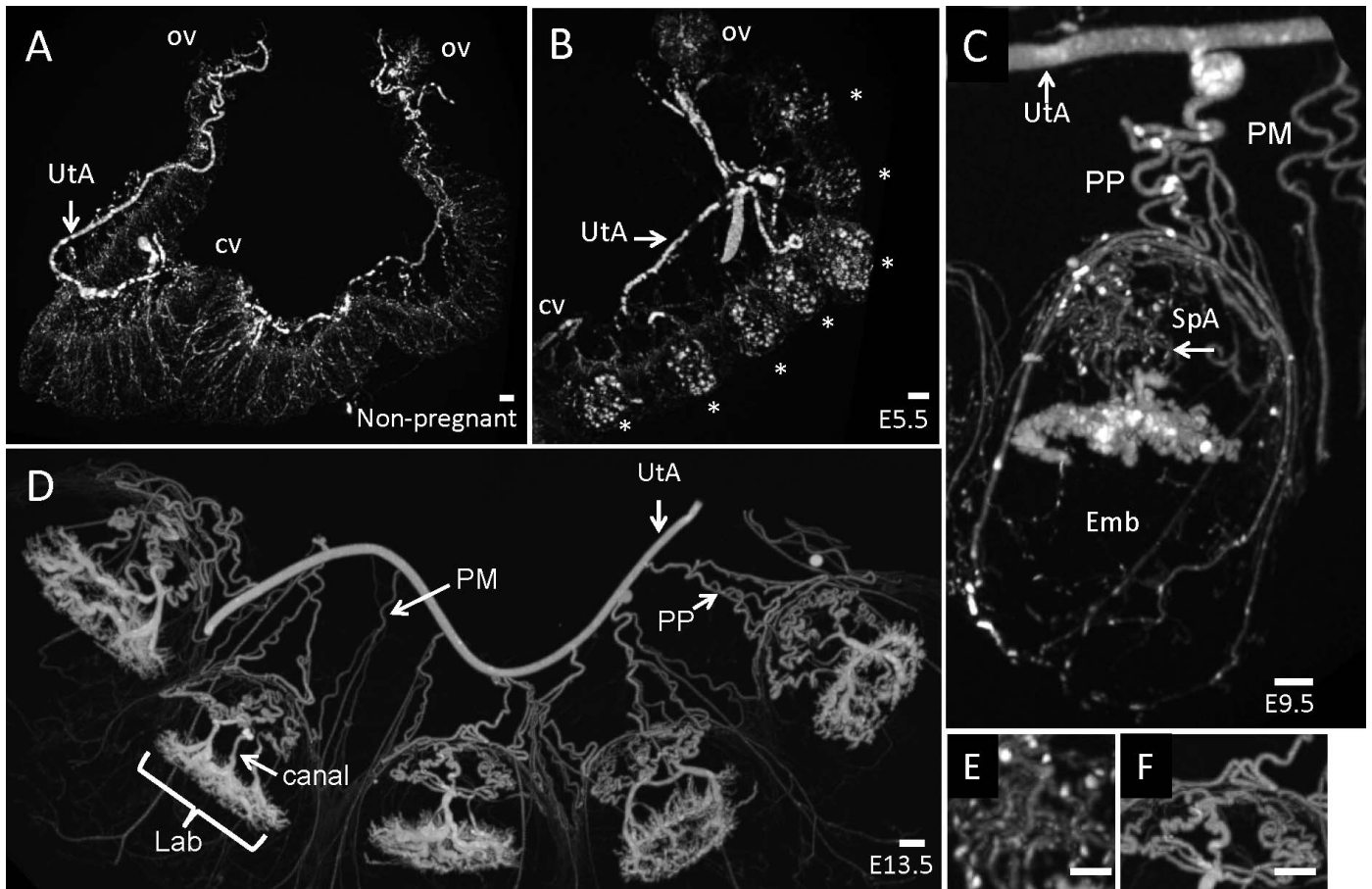
FIG. 1. Maximum intensity projection images of the uterine and uteroplacental arterial vasculature after micro-CT imaging. **A**) The nonpregnant, bicornate uterine arterial vasculature. **B**) Left horn of an E5.5 uterus with seven identifiable implantation sites (*). By E5.5, remodeling of the vasculature is present, but specific vessel types cannot yet be distinguished. **C**) This E9.5 implantation site shows distinction between the preplacental (PP) and premyometrial (PM) radial arteries. Spiral arteries (SpA) have begun to form by this stage, but canals are not yet present. **D**) Five E13.5 implantation sites. At this stage, all vessel components have formed. **E**) E9.5 spiral arteries are small in diameter with minimal coiling. By E13.5 (**F**), the spiral arteries have enlarged in diameter and taken on their characteristic coiled geometry. UtA, uterine artery; cv, cervical end of the uterus; ov, ovarian vasculature; Emb, embryonic cavity; Lab, labyrinth. Bar = 1 mm.

direct blood flow to the maternal blood spaces in the labyrinth for exchange [15].

Uterine artery augmentation was observed very early in gestation from before pregnancy to E5.5 (by 55%; Fig. 2A), after which no further significant increases were observed although there was a tendency for uterine artery diameter to increase near term. By E9.5, preplacental radial artery diameter was 30% larger than their premyometrial counterparts ($P = 0.001$), which were unchanged relative to the nonpregnant state (Fig. 2A). Interestingly, despite extensive continuing vessel growth and diameter augmentation of spiral arteries and canals, preplacental radial artery diameters did not increase after E8.5 (Fig. 2A), nor were there significant changes in the number of preplacental radial arteries (Table 1) or their vessel lengths (Table 2). Thus, enlargement of uterine and preplacental radial arteries occurred early in gestation up to onset of chorioallantoic placental exchange, which occurs at ~E9.5 [18].

Establishment and prominent enlargement of approximately seven spiral arteries and approximately three canals for each placenta (Table 1) occurred during mid- to late gestation in the mouse. Newly formed spiral arteries elongated from E9.5 to E11.5, after which their number (Table 1) and length (~8 mm) (Table 2) remained constant. Spiral artery diameter increased linearly from E9.5 throughout gestation reaching a 2-fold increase by E17.5 (Fig. 2A). This diameter increase resulted in a 4-fold increase in spiral artery cross-sectional area (Fig. 3A). By E11.5, spiral arteries fed into approximately three larger diameter canals (Fig. 2A and Table 1). The number and length of canals did not significantly increase past this point (Tables 1 and 2). However, canal diameters increased by almost 2-fold between E11.5 and E17.5 (Fig. 2A). At E13.5, large diameter canal branches appeared (Fig. 2B). There were two to six branches per implantation site that increased the number of blood flow exit points into the exchange region as well as the total vascular cross-sectional area, which enlarged by 2.5 fold from E13.5 to E17.5 (Fig. 3A). Calculated flow increased dramatically from E11.5 to E17.5 (0.8 mm³/sec at E11.5, 1.3 mm³/sec at E13.5, 3.2 mm³/sec at E15.5, 7.7 mm³/sec at E17.5), while estimated blood flow velocities from E11.5 to E17.5 were either maintained (e.g., canals) or increased (e.g., radial arteries, spiral arteries, and canal branches) (Fig. 3B).

Hemodynamic calculations based on the diameter and network arrangement of the radial arteries, spiral arteries, and maternal canals predicted a 47% drop in total arterial resistance downstream of the uterine artery from E9.5 to E17.5 (Fig. 4A). Preplacental radial arteries were the largest source of uteroplacental resistance throughout this period, accounting for over 60% of total resistance at E9.5 (Fig. 4, A and B), driven primarily by their small diameters (~100 μm; Fig. 2A) and the relatively low number of vessels in parallel (Table 1).
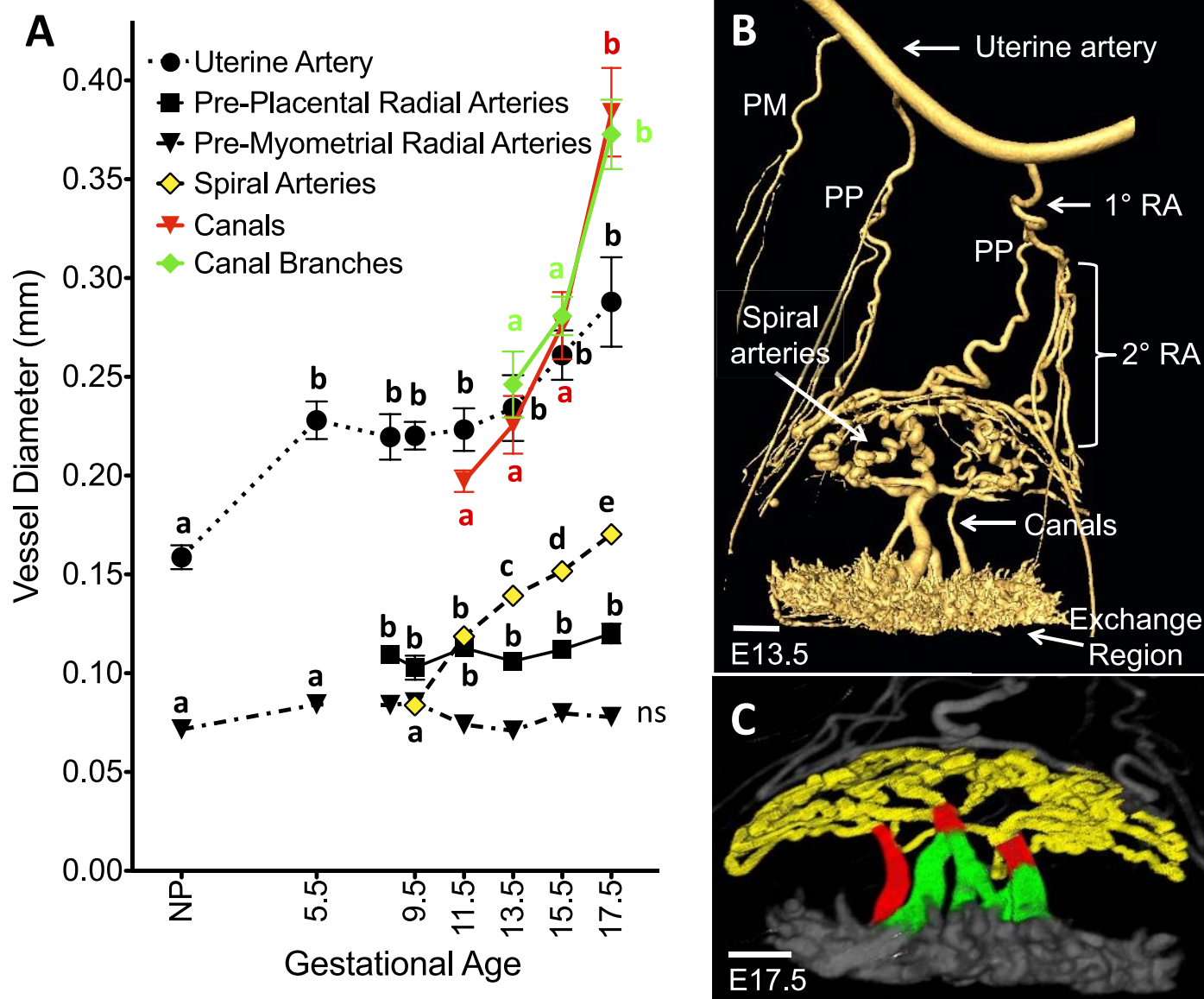
3

FIG. 2. Expansion of the uterine and uteroplacental vasculature across gestation. **A**) Uterine and uteroplacental arterial diameters in the nonpregnant uterus and across gestation. Different letters indicate significant changes with gestational age. For premyometrial radial artery and spiral artery data, the SEM error bars are smaller than the size of the data point and therefore cannot be seen. **B**) Isosurface rendering of the E13.5 uteroplacental arterial vasculature outlines tree geometry. Premyometrial (PM) and preplacental (PP) radial arteries branch from the uterine artery. Primary (1°) and secondary (2°) preplacental radial arteries (RA) feed the downstream spiral arteries and maternal canals. Basic architecture of the tree is similar at E17.5 (**C**); however, significant diameter expansion has occurred. This E17.5 image has been segmented to highlight geometry of the spiral arteries (yellow), maternal canals (red), and canal branches (green). Image from Rennie et al. [16] used with permission from Elsevier. Bar = 1 mm.

TABLE 1. Average number of vessels by type at various stages of mouse gestation.

	Stage of gestation[†]					
Vessel type*	E9.5 (n = 4)	E11.5 (n = 4)	E13.5 (n = 7)	E15.5 (n = 7)	E17.5 (n = 7)	ANOVA P
Radial artery (1°)	1.5 ± 0.3	1.8 ± 0.3	1.8 ± 0.1	1.9 ± 0.1	2.0 ± 0.2	0.57
Radial artery (2°)	3.5 ± 0.3	2.5 ± 0.3	3.6 ± 0.3	4.3 ± 0.4	4.0 ± 0.4	0.06
Spiral artery	6.8 ± 0.3	6.3 ± 0.5	7.0 ± 0.4	6.4 ± 0.2	6.6 ± 0.5	0.70
Maternal canal	0[a]	3.0 ± 0.6[b]	2.6 ± 0.3[b]	3.3 ± 0.4[b]	3.0 ± 0.3[b]	0.0001
Canal branch	0[a]	0[a]	3.7 ± 0.4[b]	4.0 ± 0.6[b]	4.0 ± 0.6[b]	0.0001

* 1° and 2°, primary and secondary radial arteries, respectively.
[†] Data are means ± SEM where n is the number of placentas analyzed.
[a,b] Different letters show a significant difference between gestational ages ($P < 0.05$) as determined by one-way ANOVA followed by Tukey post hoc tests.

TABLE 2. Average length (mm) of individual vessels by type at various stages of mouse gestation.

Vessel type*	Stage of gestation[†]					ANOVA P
	E9.5 (n = 4)	E11.5 (n = 4)	E13.5 (n = 7)	E15.5 (n = 7)	E17.5 (n = 7)	
Radial artery (1°)	1.9 ± 0.5	1.2 ± 0.3	1.9 ± 0.2	2.0 ± 0.3	2.3 ± 0.4	0.60
Radial artery (2°)	5.9 ± 0.3	6.9 ± 0.2	5.6 ± 0.6	7.7 ± 0.6	8.2 ± 0.9	0.07
Spiral artery	4.6 ± 0.3[a]	7.3 ± 0.9[b]	8.0 ± 0.4[b]	7.0 ± 0.4[b]	8.1 ± 0.6[b]	0.002
Maternal canal	N/A	1.5 ± 0.1	1.3 ± 0.1	1.5 ± 0.1	1.4 ± 0.2	0.65
Canal branch	N/A	N/A	0.9 ± 0.1	0.8 ± 0.1	1.0 ± 0.1	0.51

* 1° and 2°, primary and secondary radial arteries, respectively.
[†] Data are means ± SEM where n is the number of placentas analyzed; N/A, not applicable.
[a,b] Different letters show a significant difference between gestational ages ($P < 0.05$) as determined by one-way ANOVA followed by Tukey post hoc tests.

Due to an apparent lack of remodeling of the preplacental radial arteries after E8.5, absolute radial artery resistance did not significantly decrease in late gestation (Fig. 4A). Meanwhile, continued remodeling of the spiral arteries and maternal canals progressively decreased resistance downstream. This caused the proportion of total resistance contained in the preplacental radial arteries to increase from ~60% at E9.5 to a remarkable 91% at E17.5 (Fig. 4B). Uteroplacental blood flow, calculated from the diameter (Fig. 2A), number of canals (Table 1), and published canal blood velocities [18], was combined with preplacental radial artery resistance to estimate the pressure drop across the preplacental radial artery segment of the uteroplacental bed. Pressure drop across the radial arteries increased by more than 6-fold from E11.5 to E17.5 (Fig. 5) due to a 9-fold increase in blood flow [18] and the high level of resistance maintained in these vessels (Fig. 4A). In stark contrast to unchanging resistance in the preplacental radial arteries from E9.5 to E17.5, spiral artery resistance decreased 10-fold between E11.5 and E17.5 (Fig. 4A), such that by E17.5 the spiral arteries made up only 9% of total

uteroplacental resistance (Fig. 4B). This dramatic fall in resistance was due almost entirely to diameter enlargement of these vessels. Canals and canal branches, with diameters much larger than the spiral arteries (Fig. 2A), were negligible sources of both resistance (Fig. 4A) and pressure drop (Fig. 5). Resistance of the canal and canal branch level of the tree was 34-fold lower than that at the level of the spiral arteries (Fig. 4A). Thus, radial arteries were the predominant source of uteroplacental resistance throughout gestation, and canals contributed negligibly, whereas spiral artery enlargement was the predominant cause for the late gestational decrease in uteroplacental vascular resistance.

DISCUSSION

In this paper, we report novel information on the time course and hemodynamic consequences of de novo formed and enlarging uteroplacental arteries during pregnancy. Using high-resolution micro-CT images and geometry-based calculations of vascular resistance, we revealed vessel-type specific
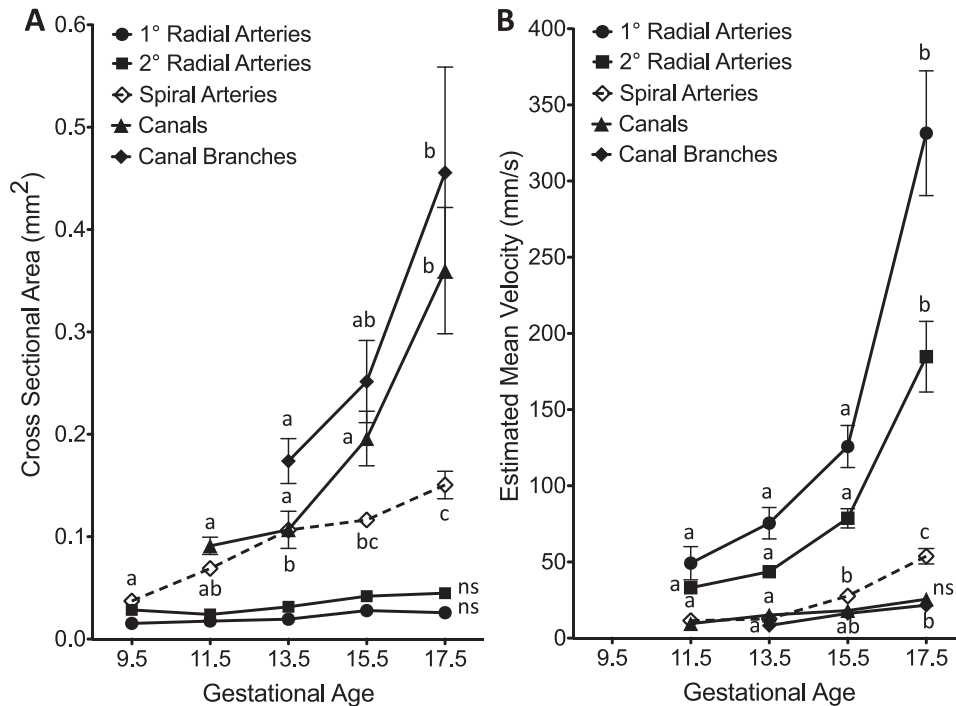

FIG. 3. Vascular cross-sectional area and mean velocities through the uteroplacental arterial tree. A) Total cross-sectional area of each vessel type was calculated across gestation based on the number of vessels and vessel diameters. B) Estimates of mean velocity were calculated from cross-sectional area data (in A) and flow velocity data (E11.5 to term [18]), assuming conservation of flow through the uteroplacental tree. Different letters indicate significant changes with gestational age. All data are shown as mean ± SEM. Some error bars are not visible because the SEM was smaller than the data point.

FIG. 4. Vascular resistance in the uteroplacental arterial tree. **A**) Vascular resistance was calculated using Poiseuille's law and standard formulas for resistances in series and parallel. **B**) The distribution of resistance in the radial arteries, spiral arteries, and canals and canal branches is plotted across late gestation. Different letters indicate significant changes with gestational age. All data are shown as mean ± SEM. Some error bars are not visible because the SEM was smaller than the data point.
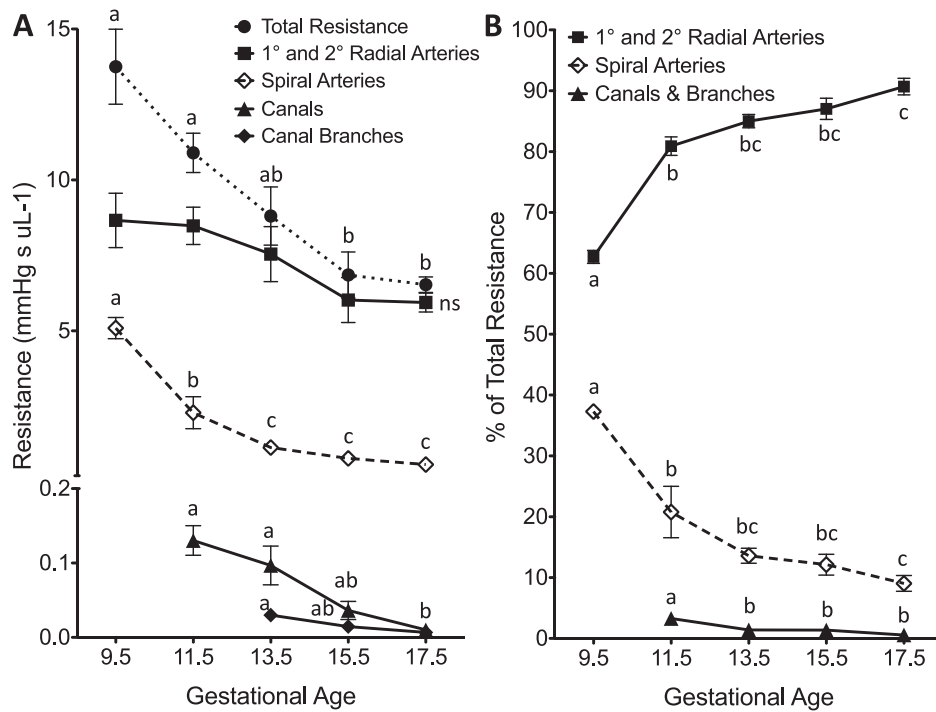

FIG. 5. Pressure gradients within the uteroplacental arterial tree. **A**) Pressure gradient was calculated from blood flow estimations and measured resistances at each level of the uteroplacental circulation. **B**) The distribution of pressure in the radial arteries, spiral arteries, and canals and canal branches is plotted across late gestation. Different letters indicate significant changes with gestational age. All data are shown as mean ± SEM. Some error bars are not visible because the SEM was smaller than the data point.
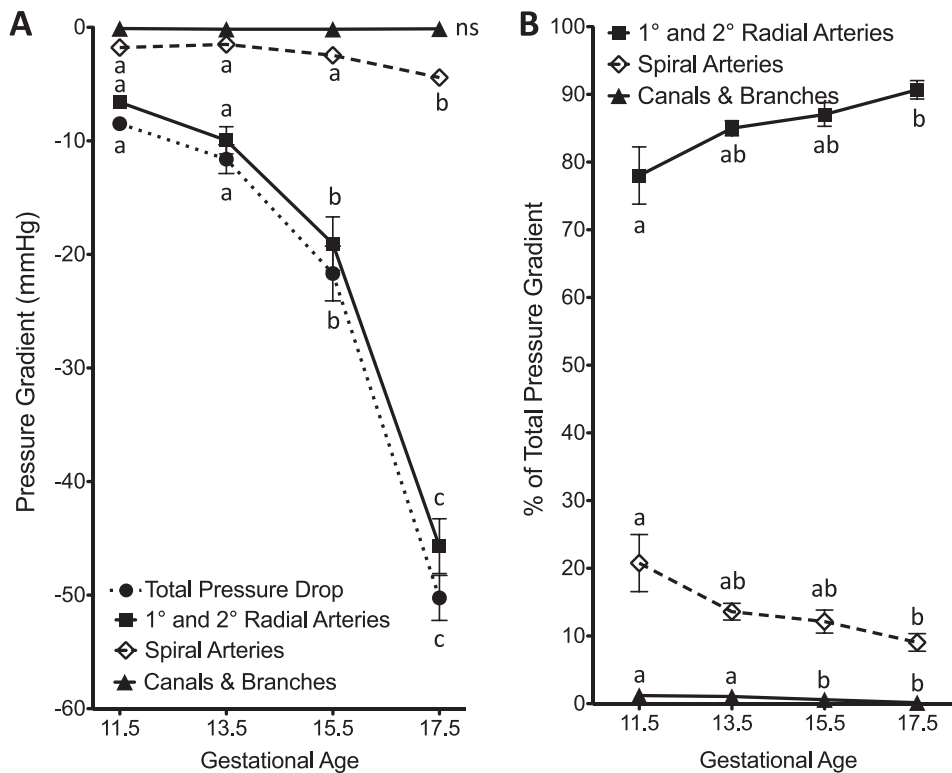
resistances and pressure drops in the uteroplacental vascular tree across mouse gestation. We observed uterine and radial artery enlargement early in gestation, seemingly anticipating large mid- and late gestational increases in uteroplacental blood flow. The decrease in vascular resistance downstream of the uterine artery from E9.5 to E17.5, calculated from vascular geometry, was in accord with predictions from in vivo uterine artery flow computed from uterine artery velocity data [18]. We found that spiral artery diameter augmentation was responsible for the overwhelming majority of the observed resistance decrease, yet data also revealed a dwarfing of absolute spiral artery resistance by that of the radial arteries. Indeed, resistance calculations highlighted the paramount importance of the radial arteries in determining total uteroplacental resistance as well as total uteroplacental pressure drop. Midgestational construction and expansion of maternal canals and canal branches augmented cross-sectional area through this region of the bed such that velocity of blood into the placental exchange region was kept low in spite of large gestational increases in blood flow.

Uterine artery diameter enlarged by E5.5, well in advance of the onset of chorioallantoic exchange at E9.5 [18, 35, 36] and also well before the onset of yolk sac exchange given that fetal vitelline perfusion does not begin until E8.5 [18]. Thus, uterine artery enlargement appears to be a pre-adaptation, likely triggered via hormonal mediators [17]. In human pregnancy, uterine artery diameter increases rapidly in early gestation: diameter increases by 70% at 16 wk [37], by 100% at 20 wk [38], and increases only a further 37% between 24 wk and term [39]. Thus, prominent uterine artery enlargement likely begins even before the onset of perfusion of the intervillous space (~12 wk [40]) in human pregnancy as well. Others surmise that in human pregnancy uterine artery enlargement appears to anticipate the large increase in uterine blood flow that occurs in later gestation [38], and our results reveal a similar phenomenon occurs in mice.

Resistance calculations based on our vessel geometry data reveal a 2.1-fold decrease in total resistance downstream of the uterine artery from E9.5 to E17.5. Vascular resistance in vivo is generally calculated from volumetric blood flow and the pressure gradient across the vessel or vascular bed. Thus, to compare our calculations with in vivo data, uterine artery blood flow velocity measurements [18] were combined with our uterine artery diameter measurements to calculate volumetric blood flow. Blood flow was thereby predicted to increase 3-fold from E9.5 to term. Maternal arterial blood pressure is unchanged over this time period in mice [41]. This flow change should therefore correspond to a 3-fold decrease in resistance. Because some of this resistance drop would presumably occur across the uterine artery, the observed 2.1-fold resistance decrease in the current study, based solely on vessel structure and geometry of uteroplacental vessels downstream of the uterine artery, is consistent with these flow measurements.

Although spiral arteries were responsible for the majority of the fall in uteroplacental resistance during pregnancy, these vessels were a minor contributor to total uteroplacental arterial resistance in late gestation. Indeed, we observed that the radial arteries dictated the vast majority of total uteroplacental resistance, reaching 90% of total resistance by E17.5. Evidence for a similar distribution of resistance in the human placenta comes from ultrasound studies in which the uterine artery was found to remain unchanged following delivery of the placenta despite shedding of the decidual spiral arteries and intervillous space [42]. Furthermore, uterine artery waveforms from abdominal pregnancies display similar changes during gestation as seen in intrauterine pregnancy, despite no possibility of

spiral artery trophoblast invasion [43, 44]. Thus, results in human pregnancy also support a negligible contribution to total uteroplacental vascular resistance by downstream vessels in the uteroplacental circulation [42–46]. Even though spiral arteries play a significant role in gestational decreases in total resistance, radial arteries are by far the largest contributor to uteroplacental resistance throughout gestation and therefore the largest determinant of uteroplacental blood flow. Given prominent similarities between the mouse and human uteroplacental vasculatures, this finding casts doubt on the prevalent view that spiral artery remodeling is the primary determinant of uteroplacental hemodynamic resistance in human pregnancies and suggests that further research in humans and other animal models is warranted.

The function of a relatively high and sustained vascular resistance in the radial arteries during pregnancy is unclear but presumably confers evolutionary benefits. High radial artery resistance would tend to promote a more even distribution of blood flow among implantation sites in litter-bearing animals like the mouse [47] as well as causing a relatively large decrement in maternal arterial pressure [45, 47]. The latter is believed to be essential to ensure that maternal pressures in the exchange region are sufficiently low that fetal capillaries, with pressures of only a few mmHg, are not collapsed [48]. Collapsed capillaries would reduce fetoplacental perfusion and thus reduce exchange. Radial arteries are also muscular [15], highly vasoactive [49], and dotted with constrictive sphincters [15]. These vessel properties likely play important roles in controlling blood flow to individual implantation sites during parturition when downstream, decidual vessels are sequentially severed while the litter is delivered. Moll and Kunzel [50] directly measured pressure in the rat uteroplacental circulation and found that the greatest pressure drop occurred across the arcuate and radial arteries. Rat and human uterine arterial anatomy differs somewhat from the mouse in that the arcuate artery, which branches from the uterine artery and gives rise to radial arteries in humans and rats [51], is not present in the much smaller circulation of the mouse. Despite this difference, if we assume pressure drop in the mouse is similar to the rat between the carotid (~100 mmHg [50]) and the spiral arteries (~10 mmHg [50]), which would include the common iliac artery, the uterine and ovarian artery cascade, and the radial arteries, our data suggest that 50% of this pressure drop (~45 mmHg) occurs across the radial arteries. The absence of late gestational radial artery expansion is especially intriguing because it suggests a complete lack of flow-mediated diameter expansion, which is the usual arterial response [52].

Uteroplacental vessel diameters and cross-sectional areas progressively increase as blood flow moves downstream, dictating that blood flow velocity progressively slows as it approaches the maternal-fetal region of exchange. Indeed, ultrasound data demonstrates blood flow velocities 40-fold slower in the canal branches (1.5 cm/sec) relative to the uterine artery (60 cm/sec) at term in the mouse [18]. If blood flow were constant, a 24-fold drop in blood velocity would be predicted based on the gestational increase in cross-sectional area of vessels entering the exchange region, from that of spiral arteries at E9.5 to canal branches at E17.5. However, after accounting for increases in blood flow between E9.5 and E17.5, the velocity of blood flow entering the placental exchange region was predicted to increase only ~2-fold. These data are in accord with the ~2-fold increase in velocity measured in vivo in maternal canals and canal branches of the mouse by microultrasound over this same gestational window [18]. The relatively small increase in velocity suggests that the large increase in cross-sectional area is tightly regulated to

offset increases in flow. Maintaining relatively low and stable flow velocities entering the exchange region over the last half of gestation is likely functionally important to promote exchange of nutrients, wastes, and gasses between the maternal and fetal circulations in the placenta as well as to reduce the risk of shear stress damage to trophoblast in the exchange region [45].

Our study reveals some strong similarities between mouse and human uteroplacental arterial expansion and the resulting fall in vascular resistance. In both species, uterine artery diameter enlarges rapidly in early gestation, well before the onset of chorioallantoic exchange in the mouse [18, 35, 36] and likely prior to perfusion of the intervillous space in humans [37, 38, 40]. This pre-adaptation of the uterine artery appears to anticipate the large increases in uterine blood flow that occur in later gestation in both species [18, 38, 53]. Early in gestation, both species also exhibit selective radial artery enlargement of preplacental but not premyometrial radial arteries [8]. Surprisingly, to our knowledge the time course of preplacental radial artery enlargement during pregnancy in humans has not been studied. Both species deliver blood into relatively open blood spaces in the exchange region via highly coiled spiral arteries and funnel-like channels, anatomy that is characteristic of the hemochorial placenta. Indeed, trophoblast-lined, distal dilations of the spiral arteries in humans augment the diameter by 5- to 6-fold [45] in a seemingly analogous way to the trophoblast-lined [15], funnel-like maternal canals and canal branches of the mouse, which we show similarly augment the terminal diameter of vessels feeding the exchange region by 4.5-fold. In addition to these similarities in vascular expansion, the calculated 47% decrease in vascular resistance in the mouse from E9.5 to E17.5 is strikingly similar to the 50% decrease in vascular resistance in the human uterine arterial circulation from mid gestation to term [53]. Similarities in uteroplacental structure, growth, and resistance in mice and humans during normal pregnancy supports the use of mouse models to discover mechanisms controlling normal uteroplacental vascular expansion and why it fails in some pathological human pregnancies [1, 6].

The novel hemodynamic insights gained from this study were possible due to the vascular perfusion, high-resolution structural imaging, and hemodynamic modeling methods presented herein; however, these methods are not without their limitations. As with all ex vivo methods requiring that vessels be filled with a contrast agent, only filled vessels are visualized and vasospasm or more subtle changes in vascular tone, both of which could affect vessel caliber, may occur. Variation in the degree of filling of the vasculature was observed at different implantation sites within the uterus with no obvious relationship with position within the horns. Incomplete filling was apparent in micro-CT images (as reported previously [33]), and these sites were not analyzed. Litter sizes were relatively large and entire uterine horns were imaged in single micro-CT scans so that implantation sites in which the contrast agent filled the entire uteroplacental tree were readily obtained for quantitative analysis. Warm perfusate containing xylocaine, a vasodilator, was used to minimize perfusion-induced changes in vascular tone and successfully avoided vasospasm in all 27 dams imaged for this study. In prior work, this perfusion method resulted in uterine and umbilical arterial diameters that did not significantly differ from in vivo measurements obtained using microultrasound [3, 33].

The vessel types that make up the uteroplacental circulation are defined based on their distinctive morphology. We show that during pregnancy vessel types also differ in the extent and time course of their morphological changes as well as in their changing hemodynamic roles. Surprisingly, most uterine and radial artery enlargement occurs very early in gestation, prior to large increases in uterine blood flow. Maternal canals and branches had a negligible effect on resistance; rather, they are seemingly analogous to terminal dilation of spiral arteries in humans [45] in maintaining low velocities to the exchange region in spite of increases in uteroplacental blood flow. Augmentation of spiral artery diameter is responsible for the overwhelming majority of the observed resistance decrease, and yet the upstream radial arteries dwarf spiral artery resistance throughout gestation. Indeed, our data support prior work showing the paramount importance of the radial arteries in determining total uteroplacental resistance, and hence blood flow, to the placenta [19, 50]. That these morphologically different vessel types differ in their remodeling responses to pregnancy may be useful in future studies using mouse models to elucidate how these processes are controlled and how vessel-specific abnormalities may contribute to pregnancy complications such as pre-eclampsia and intrauterine growth restriction. Together, current and prior results force us to question the existing dogma on the relative importance of spiral artery remodeling as a determinant of uteroplacental vascular resistance, and hence blood flow, throughout gestation in healthy and pre-eclamptic human pregnancies.

REFERENCES

1. Kaufmann P, Black S, Huppertz B. Endovascular trophoblast invasion: implications for the pathogenesis of intrauterine growth retardation and preeclampsia. Biol Reprod 2003; 69:1–7.
2. Ball E, Bulmer JN, Ayis S, Lyall F, Robson SC. Late sporadic miscarriage is associated with abnormalities in spiral artery transformation and trophoblast invasion. J Pathol 2006; 208:535–542.
3. Kulandavelu S, Whiteley KJ, Qu D, Mu J, Bainbridge SA, Adamson SL. Endothelial nitric oxide synthase deficiency reduces uterine blood flow, spiral artery elongation, and placental oxygenation in pregnant mice. Hypertension 2012; 60:231–238.
4. Verlohren S, Geusens N, Morton J, Verhaegen I, Hering L, Herse F, Dudenhausen JW, Muller DN, Luft FC, Cartwright JE, Davidge ST, Pijnenborg R, et al. Inhibition of trophoblast-induced spiral artery remodeling reduces placental perfusion in rat pregnancy. Hypertension 2010; 56:304–310.
5. Lyall F, Robson SC, Bulmer JN. Spiral artery remodeling and trophoblast invasion in preeclampsia and fetal growth restriction: relationship to clinical outcome. Hypertension 2013; 62:1046–1054.
6. Ong SS, Baker PN, Mayhew TM, Dunn WR. Remodeling of myometrial radial arteries in preeclampsia. Am J Obstet Gynecol 2005; 192:572–579.
7. Lyall F. Priming and remodelling of human placental bed spiral arteries during pregnancy–a review. Placenta 2005; 26(suppl A):S31–S36.
8. ARTS NF. Investigations on the vascular system of the placenta. II. The maternal vascular system. Am J Obstet Gynecol 1961; 82:159–166.
9. Burchell RC. Arterial blood flow into the human intervillous space. Am J Obstet Gynecol 1967; 98:303–311.
10. Cnossen JS, Morris RK, ter Riet G, Mol BW, van der Post JA, Coomarasamy A, Zwinderman AH, Robson SC, Bindels PJE, Kleijnen J, Khan KS. Use of uterine artery Doppler ultrasonography to predict pre-eclampsia and intrauterine growth restriction: a systematic review and bivariable meta-analysis. CMAJ 2008; 178:701–711.
11. Prefumo F, Sebire NJ, Thilaganathan B. Decreased endovascular trophoblast invasion in first trimester pregnancies with high-resistance uterine artery Doppler indices. Hum Reprod 2004; 19:206–209.
12. Aardema MW, Oosterhof H, Timmer A, van Rooy I, Aarnoudse JG. Uterine artery Doppler flow and uteroplacental vascular pathology in normal pregnancies and pregnancies complicated by pre-eclampsia and small for gestational age fetuses. Placenta 2001; 22:405–411.
13. Adamson SL, Langille BL. Factors determining aortic and umbilical blood flow pulsatility in fetal sheep. Ultrasound Med Biol 1992; 18:255–266.
14. Adamson SL. Arterial pressure, vascular input impedance, and resistance as determinants of pulsatile blood flow in the umbilical artery. Eur J Obstet Gynecol Reprod Biol 1999; 84:119–125.
15. Adamson SL, Lu Y, Whiteley KJ, Holmyard D, Hemberger M, Pfarrer C,

Cross JC. Interactions between trophoblast cells and the maternal and fetal circulation in the mouse placenta. Dev Biol 2002; 250:358–373.

16. Rennie MY, Mu J, Rahman A, Qu D, Whiteley KJ, Sled JG, Adamson SL. The uteroplacental, fetoplacental, and yolk sac circulations in the mouse. In: Croy BA, Yamada AT, DeMayo FJ, Adamson SL (eds.), The Guide to Investigation of Mouse Pregnancy, vol. 1, 1st ed. London, UK: Elsevier; 2014:201–210.

17. van der Heijden OW, Essers YP, Spaanderman ME, De Mey JG, van Eys GJ, Peeters LL. Uterine artery remodeling in pseudopregnancy is comparable to that in early pregnancy. Biol Reprod 2005; 73:1289–1293.

18. Mu J, Adamson SL. Developmental changes in hemodynamics of the uterine artery, the utero- and umbilico-placental, and vitelline circulations in the mouse throughout gestation. Am J Physiol Heart Circ Physiol 2006; 291:H1421–H1428.

19. Rennie MY, Rahman A, Whiteley KJ, Sled JG, Adamson SL. Site-specific increases in utero- and fetoplacental arterial vascular resistance in eNOS-deficient mice due to impaired arterial enlargement. Biol Reprod 2015; 92:48.

20. Habli M, Jones H, Aronow B, Omar K, Crombleholme TM. Recapitulation of characteristics of human placental vascular insufficiency in a novel mouse model. Placenta 2013; 34:1150–1158.

21. Doridot L, Passet B, Mehats C, Rigourd V, Barbaux S, Ducat A, Mondon F, Vilotte M, Castille J, Breuiller-Fouche M, Daniel N, le Provost F, et al. Preeclampsia-like symptoms induced in mice by fetoplacental expression of STOX1 are reversed by aspirin treatment. Hypertension 2013; 61:662–668.

22. Rennie MY, Whiteley KJ, Sled JG, Adamson SL. Scanning electron microscopy and micro-computed tomography imaging of the utero- and fetoplacental circulations. In: Croy BA, Yamada AT, DeMayo FJ, Adamson SL (eds.), The Guide to Investigation of Mouse Pregnancy, vol. 1, 1st ed. London, UK: Elsevier; 2014:637–648.

23. Venditti CC, Casselman R, Murphy MSQ, Adamson SL, Sled JG, Smith GN. Chronic carbon monoxide inhalation during pregnancy augments uterine artery blood flow and uteroplacental vascular growth in mice. Am J Physiol Regul Integr Comp Physiol 2013; 305:R939–R948.

24. Gopalakrishnan K, Mishra JS, Chinnathambi V, Vincent KL, Patrikeev I, Motamedi M, Saade GR, Hankins GD, Sathishkumar K. Elevated testosterone reduces uterine blood flow, spiral artery elongation, and placental oxygenation in pregnant rats. Hypertension 2016; 67:630–639.

25. Dokras A, Hoffmann DS, Eastvold JS, Kienzle MF, Gruman LM, Kirby PA, Weiss RM, Davisson RL. Severe feto-placental abnormalities precede the onset of hypertension and proteinuria in a mouse model of preeclampsia. Biol Reprod 2006; 75:899–907.

26. Kanasaki K, Palmsten K, Sugimoto H, Ahmad S, Hamano Y, Xie L, Parry S, Augustin HG, Gattone VH, Folkman J, Strauss JF, Kalluri R. Deficiency in catechol-O-methyltransferase and 2-methoxyoestradiol is associated with pre-eclampsia. Nature 2008; 453:1117–1121.

27. Rueda-Clausen CF, Stanley JL, Thambiraj DF, Poudel R, Davidge ST, Baker PN. Effect of prenatal hypoxia in transgenic mouse models of preeclampsia and fetal growth restriction. Reprod Sci 2014; 21:492–502.

28. Champlin AK, Dorr DL, Gates AH. Determining the stage of the estrous cycle in the mouse by the appearance of the vagina. Biol Reprod 1973; 8:491–494.

29. Byers SL, Wiles MV, Dunn SL, Taft RA. Mouse estrous cycle identification tool and images. PLoS One 2012; 7:e35538.

30. Whiteley KJ, Pfarrer CD, Adamson SL. Vascular corrosion casting of the uteroplacental and fetoplacental vasculature in mice. Methods Mol Med 2006; 121:371–392.

31. Newton DJ, McLeod GA, Khan F, Belch JJ. Mechanisms influencing the vasoactive effects of lidocaine in human skin. Anaesthesia 2007; 62:146–150.

32. Bohlen HG, Gore RW. Comparison of microvascular pressures and diameters in the innervated and denervated rat intestine. Microvasc Res 1977; 14:251–264.

33. Rennie MY, Whiteley KJ, Kulandavelu S, Adamson SL, Sled JG. 3D visualisation and quantification by microcomputed tomography of late gestational changes in the arterial and venous feto-placental vasculature of the mouse. Placenta 2007; 28:833–840.

34. Osol G, Mandala M. Maternal uterine vascular remodeling during pregnancy. Physiology (Bethesda) 2009; 24:58–71.

35. Phoon CK, Aristizabal O, Turnbull DH. 40 MHz Doppler characterization of umbilical and dorsal aortic blood flow in the early mouse embryo. Ultrasound Med Biol 2000; 26:1275–1283.

36. Cross JC, Simmons DG, Watson ED. Chorioallantoic morphogenesis and formation of the placental villous tree. Ann N Y Acad Sci 2003; 995:84–93.

37. Dickey RP, Hower JF. Ultrasonographic features of uterine blood flow during the first 16 weeks of pregnancy. Hum Reprod 1995; 10:2448–2452.

38. Palmer SK, Zamudio S, Coffin C, Parker S, Stamm E, Moore LG. Quantitative estimation of human uterine artery blood flow and pelvic blood flow redistribution in pregnancy. Obstet Gynecol 1992; 80:1000–1006.

39. Konje JC, Kaufmann P, Bell SC, Taylor DJ. A longitudinal study of quantitative uterine blood flow with the use of color power angiography in appropriate for gestational age pregnancies. Am J Obstet Gynecol 2001; 185:608–613.

40. Coppens M, Loquet P, Kollen M, De Neubourg F, Buytaert P. Longitudinal evaluation of uteroplacental and umbilical blood flow changes in normal early pregnancy. Ultrasound Obstet Gynecol 1996; 7:114–121.

41. Burke SD, Barrette VF, Bianco J, Thorne JG, Yamada AT, Pang SC, Adams MA, Croy BA. Spiral arterial remodeling is not essential for normal blood pressure regulation in pregnant mice. Hypertension 2010; 55:729–737.

42. Schaaps J-P, Tsatsaris V, Goffin F, Brichant J-F, Delbecque K, Tebache M, Collignon L, Retz MC, Foidart J-M. Shunting the intervillous space: new concepts in human uteroplacental vascularization. Am J Obstet Gynecol 2005; 192:323–332.

43. Acacio GL. Uterine artery Doppler patterns in abdominal pregnancy. Ultrasound Obstet Gynecol 2002; 20:194–196.

44. Collins SL, Grant D, Black RS, Vellayan M, Impey L. Abdominal pregnancy: a perfusion confusion? Placenta 2011; 32:793–795.

45. Burton GJ, Woods AW, Jauniaux E, Kingdom JC. Rheological and physiological consequences of conversion of the maternal spiral arteries for uteroplacental blood flow during human pregnancy. Placenta 2009; 30:473–482.

46. Everett TR, Lees CC. Beyond the placental bed: placental and systemic determinants of the uterine artery Doppler waveform. Placenta 2012; 33:893–901.

47. Egund N, Carter AM. Uterine and placental circulation in the guinea-pig: an angiographic study. J Reprod Fertil 1974; 40:401–410.

48. Karimu AL, Burton GJ. The effects of maternal vascular pressure on the dimensions of the placental capillaries. Br J Obstet Gynaecol 1994; 101:57–63.

49. D'Angelo G, Osol G. Regional variation in resistance artery diameter responses to alpha-adrenergic stimulation during pregnancy. Am J Physiol 1993; 264:H78–H85.

50. Moll W, Kunzel W. The blood pressure in arteries entering the placentae of guinea pigs, rats, rabbits, and sheep. Pflügers Archiv 1973; 338:125–137.

51. Osol G, Moore LG. Maternal uterine vascular remodeling during pregnancy. Microcirculation 2014; 21:38–47.

52. Pohl U, Holtz J, Busse R, Bassenge E. Crucial role of endothelium in the vasodilator response to increased flow in vivo. Hypertension 1986; 8:37–44.

53. Flo K, Wilsgaard T, Vartun A, Acharya G. A longitudinal study of the relationship between maternal cardiac output measured by impedance cardiography and uterine artery blood flow in the second half of pregnancy. BJOG 2010; 117:837–844.